Force Distribution Algorithms For Singularity-Free 3-DOF Parallel Haptic Device With Redundant Actuation

Tae-Ju Kim*, Goo-Bong Chung*, Byung-Ju Yi*, and Il-Hong Seo**

* School of Electrical Engineering and Computer Science, Hanyang University, Seoul, Korea
(Tel : +82-31-400-5218; E-mail: bj@hanyang.ac.kr)
**Graduate School of Information and Communication, Hanyang University, Seoul, Korea
(Tel : +82-2-2290-0392; E-mail: ihsuh@hanyang.ac.kr)

Abstract: The parallel-type mechanism provides more accurate and stiff motion than the serial-type mechanism. However, in case of using the haptic device, the performance of the force reflection can be deteriorated due to the singular points existing in workspace. In this paper, we propose a redundantly actuated parallel 3-DOF haptic device, which is singularity-free in the workspace and has an improved force reflection capability. In addition, we propose a new force distribution algorithm, which can reflect force of both high and low resolution, using two sets of actuator with different size. Redundant actuators are attached to the base frame in order to minimize the inertia of the system. Moreover, a wire and gear reduction system is employed to achieve high force reflection along with soft feeling. We confirm the performance of the force reflection capability throughout simulation.

Keywords: Redundant Actuation, Torque distribution

1. INTRODUCTION

Application of parallel mechanisms is becoming diverse in many robotic areas. Parallel mechanisms have many advantages over serial mechanism. It provides high stiffness and high accuracy as well as high payload. But it have more singular point than serial mechanism, thus it is more difficult to control than serial mechanism.[4,5,10] To cope with this problem, redundant actuation can be suggested as a means.

Redundant actuation can be easily explained in terms of mobility. Mobility of a system is defined as the number of minimum parameters, which is required to specify all the locations of the system relative to another. And it is described by

$$M = D(L-1) - \sum_{i=1}^{j} (D - F_i) \tag{1}$$

where

D : Maximum motion degree of link,

L : Number of link,

J : Number of joint,

F_i : Motion degree of i th joint.

When the number of actuators being employed is greater than M, the system is called a redundantly actuated system. Redundant actuation provides general improvement in payload, maximum velocity and acceleration. More importantly, the surplus actuators play a role of avoiding the singularity by abundant sources existing in the column space that relates the joint actuators to the output forces. General requirement of haptic device include large workspace for human operator, low apparent mass/inertia, low friction, high structural stiffness, backdriveability, absence of mechanical singularities, compactness, and so on.[1,2,9]

In this paper, we propose a methodology for simultaneous generation of coarse and fine reflection force to improve the performance of haptic devices. For this, we employ two sets of actuator with different actuator size. This method allows force reflection with both low and high resolution. In addition, using the surplus number of actuators, we propose a force distribution algorithm that can resolve the torque saturation problem.

2. KINEMATICS OF 3-DOF HAPTIC DEVICE

2.1 Geometric Description

The haptic device proposed in this paper consists of a top plate, six actuator on the base, and three serial chains connecting the top plate to the six actuators, as shown in Fig. 1. Each of the three serial chains consists of three links and three revolute joints. The length of every link is fixed to $0.1m$, and the base joint of each of the three chains is placed on the circle of radius (R) with 120° apart from each other.

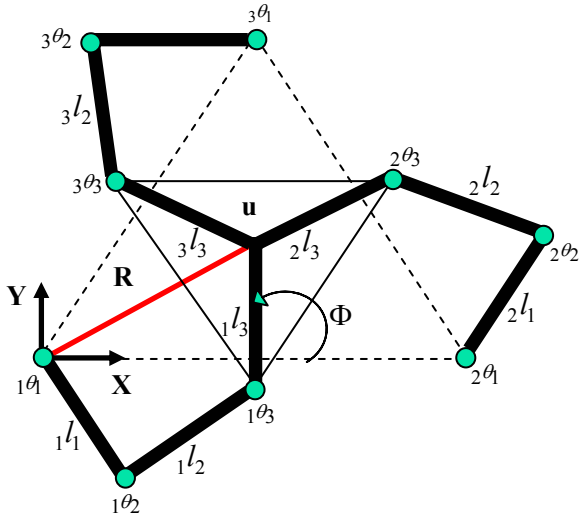

Fig. 1. 3-DOF Parallel Haptic Device

2.2 Forward Kinematics

The solution of forward kinemaitcs for each serial chain is described by Eq. (2)

$$\underline{u} = \begin{bmatrix} {}_1l_3\,{}_1C_{123} + {}_1l_2\,{}_1C_{12} + {}_1l_1\,{}_1C_1 \\ {}_1l_3\,{}_1S_{123} + {}_1l_2\,{}_1S_{12} + {}_1l_1\,{}_1S_1 \\ {}_1\theta_1 + {}_1\theta_2 + {}_1\theta_3 \end{bmatrix} \tag{2}$$

$$= \begin{bmatrix} {}_2l_3\ {}_2C_{123} + {}_2l_2\ {}_2C_{12} + {}_2l_1\ {}_2C_1 + R\sqrt{3} \\ {}_2l_3\ {}_2S_{123} + {}_2l_2\ {}_2S_{12} + {}_2l_1\ {}_2S_1 \\ {}_2\theta_1 + {}_2\theta_2 + {}_2\theta_3 \end{bmatrix}$$

$$= \begin{bmatrix} {}_3l_3\ {}_3C_{123} + {}_3l_2\ {}_3C_{12} + {}_3l_1\ {}_3C_1 + \dfrac{R\sqrt{3}}{2} \\ {}_3l_3\ {}_3S_{123} + {}_3l_2\ {}_3S_{12} + {}_3l_1\ {}_3S_1 + \dfrac{3R}{2} \\ {}_3\theta_1 + {}_3\theta_2 + {}_3\theta_3 \end{bmatrix}.$$

In the following, we describe the relationship between the operational velocity ($\dot{\underline{u}}$) and the active joint velocity ($\dot{\underline{\theta}}_A$). Differentiating Eq. (2) with respect to time gives the velocity relation, given by

$$\dot{\underline{u}} = \left[{}_1G_\phi^u \right] {}_1\dot{\underline{\phi}} = \left[{}_2G_\phi^u \right] {}_2\dot{\underline{\phi}} = \left[{}_3G_\phi^u \right] {}_3\dot{\underline{\phi}}, \quad \textbf{(3)}$$

where

$$\left[{}_iG_\phi^{u'} \right] = \left[\frac{\partial u}{\partial_i \phi_1} \quad \frac{\partial u}{\partial_i \phi_2} \quad \frac{\partial u}{\partial_i \phi_3} \right] = \left[{}_ig_1 \quad {}_ig_2 \quad {}_ig_3 \right]. \quad \textbf{(4)}$$

and

$${}_i\dot{\underline{\phi}} = \left[{}_i\dot{\phi}_1 \quad {}_i\dot{\phi}_2 \quad {}_i\dot{\phi}_3 \right]^T. \quad \textbf{(5)}$$

Eq. (3) can be rearranged according to the following form

$$\left[{}_1g_2 \quad {}_1g_3 \quad -{}_2g_2 \quad -{}_2g_2 \right] \begin{bmatrix} {}_1\dot{\phi}_2 \\ {}_1\dot{\phi}_3 \\ {}_2\dot{\phi}_2 \\ {}_2\dot{\phi}_3 \end{bmatrix} = \left[-{}_1g_1 \quad {}_2g_1 \right] \begin{bmatrix} {}_1\dot{\phi}_1 \\ {}_2\dot{\phi}_1 \end{bmatrix}, \quad \textbf{(6)}$$

$$\left[{}_2g_2 \quad {}_2g_3 \quad -{}_3g_2 \quad -{}_3g_3 \right] \begin{bmatrix} {}_2\dot{\phi}_2 \\ {}_2\dot{\phi}_3 \\ {}_3\dot{\phi}_2 \\ {}_3\dot{\phi}_3 \end{bmatrix} = \left[-{}_2g_1 \quad {}_3g_1 \right] \begin{bmatrix} {}_2\dot{\phi}_1 \\ {}_3\dot{\phi}_1 \end{bmatrix}. \quad \textbf{(7)}$$

Choosing the joints ${}_1\dot{\theta}_1$, ${}_2\dot{\theta}_1$ and ${}_3\dot{\theta}_1$ as the independent joint set ($\dot{\underline{\phi}}_a$) and the joints ${}_1\dot{\theta}_2$, ${}_1\dot{\theta}_3$, ${}_2\dot{\theta}_2$, ${}_2\dot{\theta}_3$, ${}_3\dot{\theta}_2$ and ${}_3\dot{\theta}_3$ as the dependent joint set ($\dot{\underline{\phi}}_P$). Eq. (6) and Eq. (7) can be rearranged as

$$\left[A\right] \dot{\underline{\phi}}_p = \left[B\right] \dot{\underline{\phi}}_a, \quad \textbf{(8)}$$

where

$$\left[A\right] = \begin{bmatrix} {}_1g_2 \quad {}_1g_3 \quad -{}_2g_2 \quad -{}_2g_2 & \underline{o} & \underline{o} \\ \underline{o} & \underline{o} & {}_2g_2 \quad {}_2g_3 \quad -{}_3g_2 \quad -{}_3g_3 \end{bmatrix}, \quad \textbf{(9)}$$

$$\left[B\right] = \begin{bmatrix} -{}_1g_1 \quad {}_2g_1 & \underline{o} \\ \underline{o} & -{}_2g_1 \quad {}_3g_1 \end{bmatrix}, \quad \textbf{(10)}$$

$$\dot{\underline{\phi}}_P = \left[{}_1\dot{\phi}_2 \quad {}_1\dot{\phi}_3 \quad {}_2\dot{\phi}_2 \quad {}_2\dot{\phi}_3 \quad {}_3\dot{\phi}_2 \quad {}_3\dot{\phi}_3 \right]^T, \quad \textbf{(11)}$$

and

$$\dot{\underline{\phi}}_a = \left[{}_1\dot{\phi}_1 \quad {}_2\dot{\phi}_1 \quad {}_3\dot{\phi}_1 \right]^T. \quad \textbf{(12)}$$

Now, premultiplying the matrix $\left[A\right]^{-1}$ to both sides of Eq. (8) gives the relationship between the independent joint set ($\dot{\underline{\phi}}_a$) and the dependent joint ($\dot{\underline{\phi}}_p$) :

$$\dot{\underline{\phi}}_p = \left[A\right]^{-1} \left[B\right] \dot{\underline{\phi}}_a = \left[G_a^p \right] \dot{\underline{\phi}}_a. \quad \textbf{(13)}$$

Also, the joint velocity of i th chain can be expressed in terms of the independent joint velocity

$${}_i\dot{\underline{\phi}} = \begin{bmatrix} 1 & 0 & 0 \\ \left[G_a^p \right]_{1j} \\ \left[G_a^p \right]_{2j} \end{bmatrix} \begin{bmatrix} {}_1\dot{\phi}_1 \\ {}_2\dot{\phi}_1 \\ {}_3\dot{\phi}_1 \end{bmatrix} = \left[{}_iG_a^\phi \right] \dot{\underline{\phi}}_a. \quad \textbf{(14)}$$

Substituting Eq. (14) into Eq. (3) yields the following relationship between the velocity of end-effector and the independent joint velocity

$$\dot{\underline{u}} = \left[G_a^u \right] \dot{\underline{\phi}}_a, \quad \textbf{(15)}$$

where

$$\left[G_a^u \right] = \left[{}_iG_\phi^u \right] \left[{}_iG_a^\phi \right]. \quad \textbf{(16)}$$

By inverting Eq. (15), we obtain

$$\dot{\underline{\phi}}_a = \left[G_u^a \right] \dot{\underline{u}}. \quad \textbf{(17)}$$

Choosing the joints ${}_1\dot{\theta}_1$, ${}_1\dot{\theta}_2$, ${}_2\dot{\theta}_1$, ${}_2\dot{\theta}_2$, ${}_3\dot{\theta}_1$ and ${}_3\dot{\theta}_2$ as the active joints set ($\dot{\underline{\phi}}_A$), we have a relationship between the active joints and the independent joints :

$$\dot{\underline{\phi}}_A = \left[G_a^A \right] \dot{\underline{\phi}}_a, \quad \textbf{(18)}$$

where

$$\left[G_a^A \right] = \begin{bmatrix} 1 & 0 & 0 \\ \left[G_a^P \right]_{1j} \\ 0 & 1 & 0 \\ \left[G_a^P \right]_{3j} \\ 0 & 0 & 1 \\ \left[G_a^P \right]_{5j} \end{bmatrix}. \quad \textbf{(19)}$$

Substituting Eq. (17) into Eq. (18) yields the following relationship between the active joint velocity and the velocity of end-effector

$$\dot{\underline{\phi}}_A = \left[G_a^A \right] \left[G_u^a \right] \dot{\underline{u}} = \left[G_u^A \right] \dot{\underline{u}}. \quad \textbf{(20)}$$

According to the duality existing between the velocity vector and the force vector, the following relationship exists.

$$\underline{T}_u = \left[G_u^A \right]^T \underline{T}_A, \quad \textbf{(21)}$$

where $\underline{T}_u$ denotes the output force vector and $\underline{T}_A$ denotes the joint torque vector.

2.3 Algorithm

In case of using haptic device with non-redundant actuation, it is sometime hard to generate a high torque and high force resolution to reflect a high force and accurate force at the end-effector. However, in case of using redundant actuation, a high and accurate force can be achieved by employing two sets of actuator with different sizes and using several force distribution algorithms. The proposed 3-DOF haptic mechanism is driven by 6 actuators; three on the base location and three on the second joint location. We select the base

actuators as high power device with low resolution and the floating actuators are on the reverse. The particular solution of Eq. (21) given by

$$\underline{T}_A = \left(\left[G_u^A \right]^T \right)^+ \underline{T}_u . \tag{22}$$

implies a minimum norm solution.

To reflect force of both high and low resolution, the force felt in end-effector must be distributed to base actuators and floating actuators according to some fashion. Using weighted pseudo-inverse is one way. The weighted pseudo-inverse is given by

$$\left(\left[G_u^A \right]^T \right)^+ = [W]^{-1} \left[G_u^A \right] \left(\left[G_u^A \right]^T [W]^{-1} \left[G_u^A \right] \right)^{-1}, \tag{23}$$

where

$$[W] = \begin{bmatrix} w_1 & 0 & 0 & 0 & 0 & 0 \\ 0 & w_2 & 0 & 0 & 0 & 0 \\ 0 & 0 & w_3 & 0 & 0 & 0 \\ 0 & 0 & 0 & w_4 & 0 & 0 \\ 0 & 0 & 0 & 0 & w_5 & 0 \\ 0 & 0 & 0 & 0 & 0 & w_6 \end{bmatrix}. \tag{24}$$

The magnitude of weighting factors can be decided according to the size of actuators. For instance, the weighting factors for the base actuators and the floating actuator can be given as

$$w_{1,3,5} = \frac{K_1}{\Delta F}, \quad w_{2,4,6} = \frac{K_2}{\Delta F}, \tag{25}$$

where K_1 and K_2 are scaling factors and ΔF denote the variation of the output force.[8]

If the torques of floating actuators, which is calculated by solving Eq. (23), is over the torque limit, we need to employ a new solution by using nullspace [3,8], given by

$$\underline{T}_A = \left(\left[G_u^A \right]^T \right)^+ \underline{T}_u + \left(I - \left(\left[G_u^A \right]^T \right)^+ \left(\left[G_u^A \right]^T \right) \right) \underline{\varepsilon} . \tag{26}$$

Assuming the i th floating actuator is over the torque limit, we can set the torque of the saturated joint as a fixed value and then distribute the burden to the other actuators. It can be done by employing

$$[G]^T \underline{T}_A = T_{\max}, \tag{27}$$

where $[G]$ is a vector in which the i th element is 1, and the others is 0.

Substituting Eq. (27) into Eq. (28) yields the following equation

$$\begin{aligned} T_{\max} &= [G]^T \underline{T}_A = [G]^T \left(\left[G_u^A \right]^T \right)^+ \underline{T}_u \\ &+ [G]^T \left(I - \left(\left[G_u^A \right]^T \right)^+ \left(\left[G_u^A \right]^T \right) \right) \underline{\varepsilon} . \end{aligned} \tag{28}$$

Therefore, the vector $\underline{\varepsilon}$ can be obtained as

$$\underline{\varepsilon} = [C]^+ \left(T_{\max} - [G]^T \left(\left[G_u^A \right]^T \right)^+ \underline{T}_u \right), \tag{29}$$

where

$$[C] = [G]^T \left(I - \left(\left[G_u^A \right]^T \right)^+ \left(\left[G_u^A \right]^T \right) \right). \tag{30}$$

Substituting Eq. (30) into Eq. (27) yields a new solution, which takes into account the torque limit.

$$\begin{aligned} \underline{T}_A &= \left(\left[G_u^A \right]^T \right)^+ \underline{T}_u + \left(I - \left(\left[G_u^A \right]^T \right)^+ \left(\left[G_u^A \right]^T \right) \right) [C]^+ \\ &\left(T_{\max} - [G]^T \left(\left[G_u^A \right]^T \right)^+ \underline{T}_u \right). \end{aligned} \tag{31}$$

3. SIMULATION ENVIRONMENT

Fig. 2 illustrates a virtual simulator that consists of a rectangular wall and a moving object. This simulation is performed by using Visual C++ 6.0 with OpenGL on the Windows NT environment. The white box is an object, which is being moved by the user's command from the haptic device. The square, which is modeled as a wall having elasticity, restricts the motion of the moving object. When the collision between the object and the wall occurs, the reflecting force is computed.

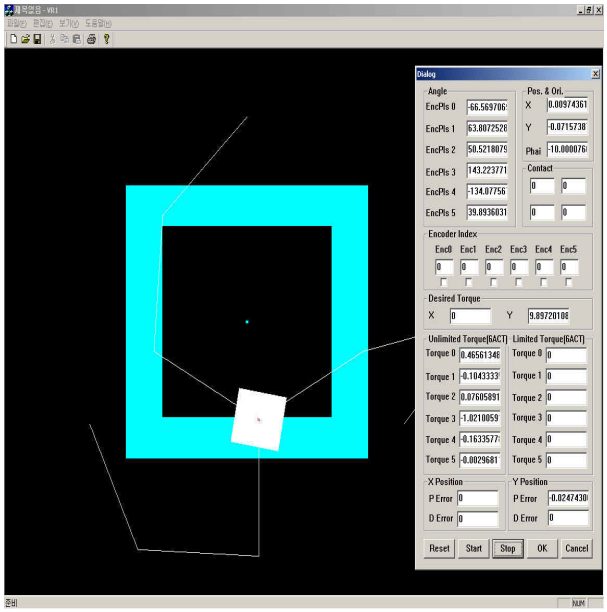

Fig. 2 Graphic Simulator

4. SIMULATION RESULT

Haptic device generates reflecting force according to the situation of virtual environment. Collision between the object and the environment causes reflection force. Several algorithms to compute actuating torque for those reflection forces are tested and compared in this section.

4.1 Comparison of Minimum Norm Solution and Weighted Pseudo-Inverse Solution

When a moving object collides with the wall, the reflecting force to restrict the operator's motion has to be generated. Fig. 3 illustrates the desired force profile required at the end position.

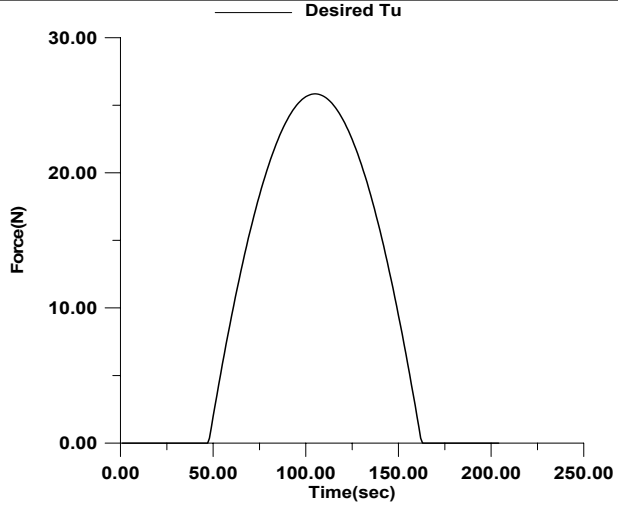

Fig. 3 Desired Force (T_u)

Specifically, Fig. 4 shows the torque profile of a base actuator (M1;line with point) and a floating actuator (M2;solid line) to satisfy a reflecting force that is given by Fig. 3. This solution is computed from Eq. (22).

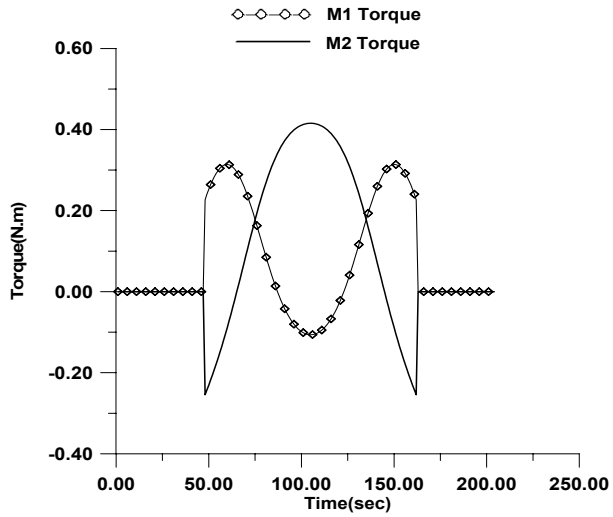

Fig. 4 The torque values of actuator M1 and M2

Though this solution shows minimum torque norm, high torque is observed at the floating actuator(M2) of small size, which will cause torque saturation at the floating actuator(M2).

For more efficient distribution of actuating torque, weighted pseudo-inverse algorithm is employed. The base motor(M1) takes on large torque and the floating actuator(M2) takes on smaller torque to avoid saturation.

Fig. 5 illustrates the torque calculated by using weighed pseudo inverse. It can be seen that the torque of the floating actuator becomes smaller, enough to avoid saturation. Thus, the weighted pseudo-inverse algorithm can be used as an effective means to avoid saturation.

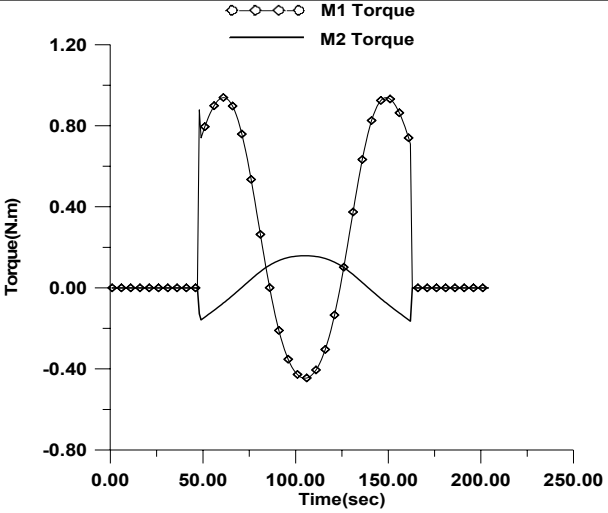

Fig. 5 The torque values of actuator M1 and M2

4.2 Comparison of Weghted Pseudo-Inverse Solution and Force Distribution Algorithm with Consideration of Torque Limit

Even when employing weighted pseudo inverse algorithm, floating actuators still can be saturated. In this case, we can set the torque of floating actuator as a fixed value and distributes the burden to the other actuators by using nullspace. When employing the weighted pseudo-inverse solution, Fig. 6 illustrates the torque of a base actuator(M3) and a floating actuator(M4) to generate a force that is given by Fig. 3. Despite of employing weighted pseudo inverse, this case shows that the torque of floating actuator is over the torque limit. (for instance, $0.4Nm$)

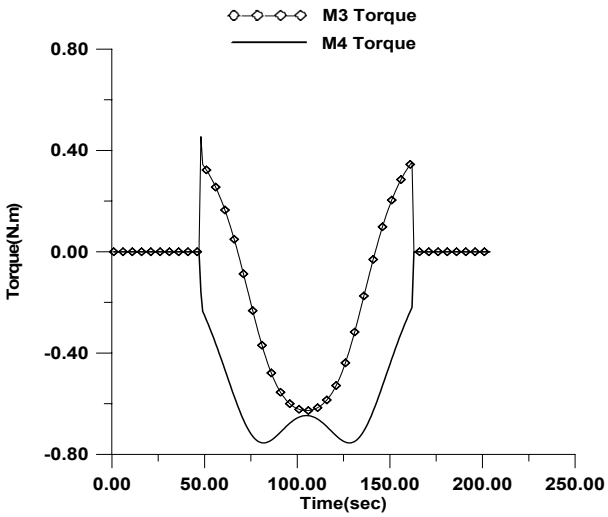

Fig. 6 The torque values of actuator M3 and M4

To resolve this problem, the nullspace solution given in Eq. (26) is employed. As shown in Fig. 7 when the torque of floating actuator is fixed as $0.4Nm$, the burden is distributed to the other actuators without any additional torque saturation.

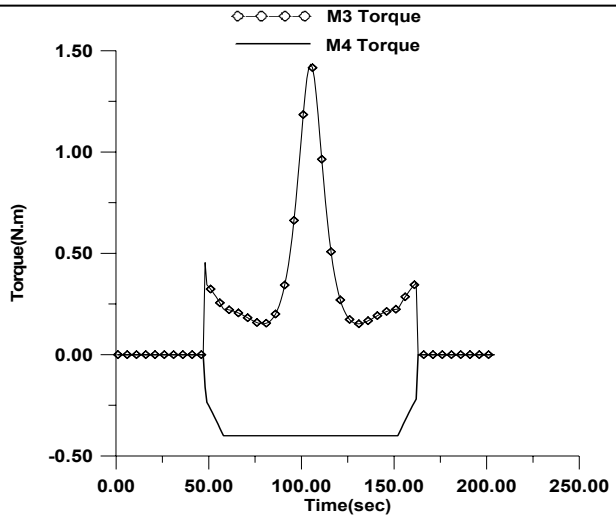

Fig. 7 The torque values of actuator M3 and M4

As shown in Fig. 6 and Fig. 7, redistribution of the system load by using the nullspace is effective to ensure avoidance of torque saturation along with satisfying the desired reflecting force at the end-position.

5. CONCLUSION

In this work, we proposed a new force distribution algorithm in which reflecting force of both high and low resolution is achievable by using two sets of actuator with different size. Minimum norm solution, weighted pseudo inverse algorithm, and a force distribution algorithm considering torque limit are investigated. Conclusively, combination of weighted pseudo inverse algorithm and a force distribution considering torque limit allows the force reflection of both high and low resolution. Currently, experimental verification of the proposed load distribution algorithms are being conducted. Fig 8 shows the prototype of 3-DOF haptic device for experimentation.

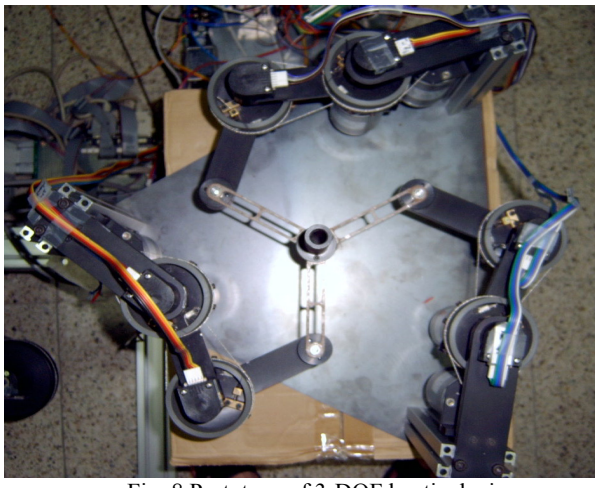

Fig. 8 Prototype of 3-DOF haptic device

REFERENCES

[1] Jae Hoon Lee, et al. "Design Scheme for a 6-DOF Parallel Haptic Device and Comparative Study on the Singularity-Free Algorithms," *Journal of Control, Automation and Systems Engineering*, Vol. 8, No. 12, pp. 1041-1047, 2002.

[2] Jae Hoon Lee, et al. "A New 6-DOF Parallel Haptic Device : Optimum Design and Analysis," *Journal of Control, Automation and Systems Engineering*, Vol. 9, No. 1, pp. 63-72, 2003.

[3] John M. Hollerbach and KI C. SUH, "Redundancy Resolution of Manipulators through Torque Optimization," *Journal of Robotics and Automation* , Vol. RA-3, No. 4, pp. 308-316, August 1987.

[4] Clement Gosselin, et al. "The Optimum Kinematic Design of a Planar Three-Degree-of-Freedom Parallel Manipulator," *Journal of Mechanisms, Transmissions, and Automation in Design* ,Vol. 110, pp. 35-41, 1988.

[5] Kuk Hoon Cho, et al. "Parallel Gripper Mechanism," *Journal of the Korean Society of Precision Engineering* ,Vol. 16, No. 11, pp. 89-97, 1999.

[6] Sang Heon Lee, et al. "Control of Active Stiffness and Impact Disturbance by Redundancy Actuated Mechanism, " *Ph,D. Dissertation*, Department of Mechanical Engineering, Kaist, 2000.

[7] Sang Heon Lee, et al. "Performance Analysis and Optimal Actuator Sizing for Anthropomorphic Robot Modules with Redundant Actuation," *KSME*, Vol. 19, No. 1 , pp. 181-192, 1995.

[8] Yoshihiko Nakamura, *Advanced Robotics: Redundancy and Optimization*, Addison-Wesley Publishing Company, 1991.

[9] R.E. Ellis, O.M. Ismaeil, and M.G. Lipsett, "Design and Evaluation of High-Performance Haptic Interface," *Robotica*, Vol. 4, 1996

[10] M. Sklar and D. Tesar, "Dynamic Analysis of Hybrid Serial Manipulator Systems Containing Parallel Modules," *Journal of Mechanisms, Transmissions, and Automation in Design*, Transactions of the ASME, pp 1-7, 1986.